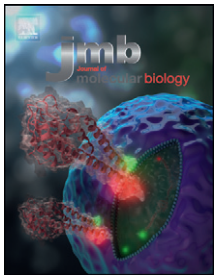

The N-Terminal Sequence of Tyrosine Hydroxylase Is a Conformationally Versatile Motif That Binds 14-3-3 Proteins and Membranes

Åge Aleksander Skjevik[1,†], Mauro Mileni[2], Anne Baumann[1], Øyvind Halskau[3], Knut Teigen[1], Raymond C. Stevens[2] and Aurora Martinez[1]

*1 - **Department of Biomedicine,** University of Bergen, Jonas Lies vei 91, 5009 Bergen, Norway*
*2 - **Department of Molecular Biology,** The Scripps Research Institute, 10550 North Torrey Pines Road, La Jolla, CA 92037, USA*
*3 - **Department of Molecular Biology,** University of Bergen, Thormøhlensgate 55, N-5020 Bergen, Norway*

Correspondence to Aurora Martinez: *aurora.martinez@biomed.uib.no*
http://dx.doi.org/10.1016/j.jmb.2013.09.012
Edited by J. Bowie

Abstract

Tyrosine hydroxylase (TH) catalyzes the rate-limiting step in the synthesis of catecholamine neurotransmitters, and a reduction in TH activity is associated with several neurological diseases. Human TH is regulated, among other mechanisms, by Ser19-phosphorylation-dependent interaction with 14-3-3 proteins. The N-terminal sequence (residues 1–43), which corresponds to an extension to the TH regulatory domain, also interacts with negatively charged membranes. By using X-ray crystallography together with molecular dynamics simulations and structural bioinformatics analysis, we have probed the conformations of the Ser19-phosphorylated N-terminal peptide [THp-(1-43)] bound to 14-3-3γ, free in solution and bound to a phospholipid bilayer, and of the unphosphorylated peptide TH-(1-43) both free and bilayer bound. As seen in the crystal structure of THp-(1-43) complexed with 14-3-3γ, the region surrounding pSer19 adopts an extended conformation in the bound state, whereas THp-(1-43) adopts a bent conformation when free in solution, with higher content of secondary structure and higher number of internal hydrogen bonds. TH-(1-43) in solution presents the highest mobility and least defined structure of all forms studied, and it shows an energetically more favorable interaction with membranes relative to THp-(1-43). Cationic residues, notably Arg15 and Arg16, which are the recognition sites of the kinases phosphorylating at Ser19, are also contributing to the interaction with the membrane. Our results reveal the structural flexibility of this region of TH, in accordance with the functional versatility and conformational adaptation to different partners. Furthermore, this structural information has potential relevance for the development of therapeutics for neurodegenerative disorders, through modulation of TH–partner interactions.

Introduction

Tyrosine hydroxylase (TH) catalyzes the hydroxylation of L-tyrosine (L-Tyr) to L-3,4-dihydroxyphenylalanine (L-Dopa), using the cofactor tetrahydrobiopterin (BH_4) and dioxygen as additional substrate. L-Dopa is the precursor of the catecholamines dopamine, noradrenaline and adrenaline, which act as neurotransmitters in the central nervous system and as hormones in the neuroendocrine system, where noradrenaline and adrenaline secreted by the chromaffin cells from the medulla of the adrenal gland initiate the fight-or-flight response. A decrease in TH activity is associated with many neuropsychiatric and neurodegenerative diseases such as Dopa-responsive dystonia, Parkinson's and Alzheimer's disease and others. The enzyme is thus strictly regulated both at the transcriptional and posttranscriptional level [1–3].

Short-term changes in TH activity and regulation of the synthesis of dopamine appear to be associated with posttranscriptional modifications in a sequence stretch located at the N-terminus of the protein, adjacent to the regulatory ACT domain. This

sequence includes four phosphorylation sites (Thr8, Ser19, Ser31 and Ser40 in human TH isoform 1) that are phosphorylated by different kinases, with considerable specificity for each site [2,3]. Thus, these phosphorylation events involve the N-terminal sequence, but little structural information is available on the conformational changes associated with each specific modification. Phosphorylation of Ser40 by cAMP-dependent protein kinase is the most studied event, both *in vitro* and *in vivo* [2,3]. This phosphorylation activates the enzyme and also counteracts the feedback inhibition of TH by catecholamines, an inhibition that is competitive with respect to the cofactor BH_4. Hydrogen/deuterium exchange [4] and fluorescence spectroscopy [5] have revealed a more open conformation for Ser40-phosphorylated TH, with a higher exposure of regions Ile35-Leu41 and Ile42-Ala71 [4]. The first region includes the recognition site for cAMP-dependent protein kinase (residues Arg37 and Arg38), and at the same time it plays a key role in determining the inhibition by dopamine [6,7]. Phosphorylation at Ser19 by p38-regulated/activated kinase and by Ca^{++}/calmodulin-dependent protein kinase II activates and stabilizes TH through a mechanism that requires the binding to 14-3-3 proteins [2,3,8]. Conformational changes related to Ser19 phosphorylation are not so well understood, but time-resolved tryptophan fluorescence and circular dichroism (CD) measurements revealed that Ser19 phosphorylation and binding to 14-3-3 reduced the solvent exposure of residues 14 and 34 and also reduced the sensitivity of the N-terminal part of TH (first 33 residues) toward proteolysis [9]. However, neither phosphorylation nor the binding to 14-3-3 proteins appeared to significantly change the secondary structure of the regulatory domain [9]. Finally, the effect of phosphorylation of Thr8 and Ser31 by other kinases such as ERK and Cdk5 is much less understood, but their influence in the regulation of TH activity and dopamine synthesis is starting to be elucidated [10,11].

TH is essentially soluble and cytoplasmic, but a fraction is also found as membrane bound in the brain, notably at nerve endings and synaptic vesicles [12–15]. Little is known about the significance of the interaction of TH with membranes, but it has been speculated that it could contribute to modulate the distribution of TH in the cytoplasm and the membrane fractions, and coordinate dopamine synthesis and packaging in the vesicles [14,16]. Recent studies have shown that the association of TH with synaptic vesicles might occur through the formation of a complex with the vesicular monoamine transporter 2 and aromatic amino acid decarboxylase [17]. However, a direct interaction of TH with the membrane has been demonstrated both with chromaffin granule membranes [18] and with synthetic phospholipid bilayers [19], and it might be hypothesized that this direct association has a cytotoxic effect, as found for other protein:membrane interactions involved in neurodegeneration [20,21]. With respect to protein motifs involved in the interaction of the enzyme with the membrane, it has been shown that truncated forms of the recombinant human TH isoform 1 lacking up to residues 33–49 do not bind to membranes [19]. Moreover, the peptide TH-(1-43), corresponding to the N-terminal sequence of TH (residues 1–43), binds to negatively charged membranes [22] and, as seen by surface plasmon resonance (SPR), the unphosphorylated TH-(1-43) peptide showed higher affinity for negatively charged membranes than the Ser19-phosphorylated THp-(1-43) peptide [22]. However, little is known about the structural determinants and conformational changes associated with membrane binding. On the other hand, THp-(1-43) showed, as expected, a much higher affinity for 14-3-3γ (K_d = 0.5 μM) than the unphosphorylated counterpart (K_d = 1550 μM) [22]. The structure–energetics relationships for the complex formation between 14-3-3 proteins and a number of phosphopeptides are relatively well understood from crystal structure analyses of several complexes [23–26]. The phosphorylated 14-3-3-interacting proteins and peptides customarily present three binding motifs: RSXpSXP (mode I), RX(Y/F)XpSXP (mode II) and carboxy-terminal (pS/pT)X1–2-COOH (mode III), where X is not Pro [27]. The TH sequence that binds to 14-3-3 proteins does not conform to these consensus motifs.

The structural analysis of full-length TH has been unattainable so far, and only the catalytic and oligomerization domains have been crystallized [28]. Thus, there is no structural information on neither the regulatory ACT domain nor its N-terminal extension that includes residues 1–43. While the regulatory ACT domain is characteristic of the four mammalian aromatic amino acid hydroxylases, an N-terminal extension of similar length is present in neuronal tryptophan hydroxylase isoform 2 (TPH2) [29,30] but not in phenylalanine hydroxylase and TPH1. The TPH2 extension does not show sequence similarity with its TH counterpart, yet it has a similar 14-3-3-interacting phosphorylatable site at Ser19 [29,31].

In this work, we have studied the conformation of the unphosphorylated TH-(1-43) and Ser19-phosphorylated THp-(1-43) N-terminal peptides in three states, that is, bound to 14-3-3γ, unbound in solution and bound to negatively charged bilayers. Through integration of several experimental (X-ray crystallography, CD and SPR) and computational methods [molecular dynamics (MD) simulations and energetic decomposition analysis by molecular mechanics Poisson–Boltzmann surface area (MM/PBSA)], we investigated the conformational change effected by phosphorylation at Ser19 and the structural determinants for interaction of THp-(1-43) with 14-3-3γ and of both TH-(1-43) and THp-(1-43) with negatively charged bilayers. These detailed analyses

reveal the conformational versatility of this N-terminal regulatory region in TH and provide a structural frame for attempts to develop drugs that stabilize/disrupt interactions with 14-3-3 proteins and membranes.

Results and discussion

The conformation of THp-(1-43) bound to 14-3-3γ

In order to identify the structural determinants for interaction of Ser19-phosphorylated TH with 14-3-3γ, we determined the crystal structure of 14-3-3γ with THp-(1-43) (PDB code 4J6S; crystallographic statistics in Table 1). The structure was solved by molecular replacement using the structure of dimeric 14-3-3γ (PDB code 2B05) as a model. The final model included four chains in the asymmetric unit (A–D) (Fig. 1a). The dimers were almost identical [RMSD for Cα atoms of chains A,B (dimer 1) and chains C,D (dimer 2) is 0.481 Å]. Furthermore, in the final model the THp peptide in complex with 14-3-3γ adopts an extended conformation, similar to previously solved structures of peptides bound to 14-3-3γ, which adopt an extended conformation, such as PDB code 2B05 (RMSD for Cα atoms for chains A,B in both structures, 0.827 Å) and PDB code 3UZD (RMSD = 1.504 Å) [59]. The structure superimposed with PDB code 2B05 is shown in Fig. 1b. The present structure of 14-3-3γ extends to residue Asp239, that is, five residues longer than the other available structures, and reveals the start of the C-terminal stretch, which seems to adopt a random-coil configuration (Fig. 1b). This stretch has been found to have an important regulatory role and folds into the phosphopeptide binding site in the absence of ligand, while it is released in the ligand-bound state [60,61]. The phosphorylated TH peptide included in the model

Table 1. X-ray crystallographic statistics for the 14-3-3γ: THp-(1-43) complex structure (PDB code 4J6S). Values in parenthesis are referring to highest resolution shell data

Crystal data	
Space group	$P2_12_12_1$
Cell dimensions	
a, *b*, *c* (Å)	84.19, 115.12, 136.90
α, β, γ, (°)	90.0, 90.0, 90.0
Data collection	
Processing software	XDS
Wavelength (Å)	1.0331
Resolution (Å)	40.0–3.08 (3.16–3.08)
R_{merge} (%)	11.1 (49.2)
$I/\sigma I$	11.6 (3.3)
Completeness (%)	87.1 (90.0)
Number of unique reflections	22,015
Redundancy	5.1 (5.1)
Refinement	
Processing software	Refmac 5
Resolution (Å)	3.08 (3.16–3.08)
Reflections	20,915 (1565)
R_{work}/R_{free} (%)	21.0 (28.1)/25.4 (36.4)
Number of atoms	7970
14-3-3γ protein	7690
THp peptide fragment	280
Average *B* overall (Å^2)	69.7
14-3-3γ protein	69.0
THp peptide fragment	86.2
RMSD bond length (Å)	0.009
RMSD bond angle (°)	1.192
PDB entry	4J6S

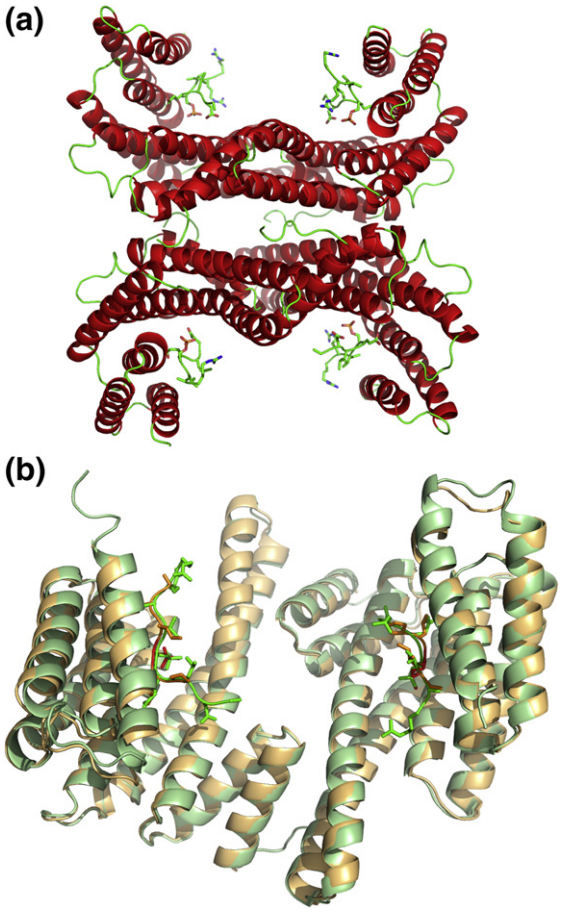

Fig. 1. The crystal structure of 14-3-3γ bound to the THp fragments. (a) The two 14-3-3γ dimers (chains A–D) in the asymmetric unit (from this work; PDB code 4J6S) represented as ribbons colored by secondary structure, complexed to the TH peptides represented by sticks. (b) A dimer of 14-3-3γ (chains A and B in PDB code 4J6S), as pale-green ribbons, with the TH peptides as bright-green sticks, superimposed with the equivalent dimeric structure of 14-3-3γ from PDB code 2B05, as pale-orange ribbons, with the phosphopeptide (RAIpSLP) represented by ocre sticks.

(PDB code 4J6S) consisted of residues RRAVp-SELDA. This sequence does not totally concur with the consensus binding modes of 14-3-3 partner proteins [24,25,27]. The positioning and conformation of the observed fragment of THp-(1-43) is nevertheless similar to that of the model peptide in PDB code 2B05 (RAIpSLP), which belongs to the canonical mode I motif (Fig. 1b; see also below).

For the MD simulation, we used a template where, by implementing weaker portions of the electron density for modeling, the THp fragment residues were extended to 12 and 13 residues in the two monomers, respectively. More specifically, the final model consisted of a 14-3-3γ dimer with a THp-(1-43) peptide fragment bound to each monomer, one with residues Phe14-Ala26 and the other with residues Ala11-Asp22 (System A in Table 2). The simulated system was divided into two receptor:ligand pairs prior to MM/PBSA analysis, each unit consisting of a 14-3-3γ monomer with bound phosphorylated TH peptide fragment. A representative snapshot of the 14-3-3γ:THp system along with close-ups of the most important hydrogen bond interactions taking place between the THp fragments and 14-3-3γ are depicted in Fig. 2a–c.

MM/PBSA decomposition analyses were performed in order to obtain more detailed information on the interactions between the THp peptide fragments and 14-3-3γ. Table 3 presents the total binding enthalpy ($\Delta G'$) decomposed into its component energy terms given in Eq. (4) (Materials and Methods). For simplicity, the polar energy terms were summed into a total polar contribution. ΔE_{elec}, the electrostatic term calculated from the force field, makes a very favorable contribution while ΔG_{PB} makes an equally unfavorable contribution to the binding enthalpy. Their opposing effects on the enthalpic energy change and comparable sizes render the sum of them more informative than the large individual contributions.

The non-polar desolvation energy ($\Delta G_{non\text{-}polar}$) is not decomposable for MM/PBSA using the MMPBSA.py implementation of AmberTools 1.5 [44]. It is therefore not included in the ΔG_{decomp} energies featured in Fig. 3, which shows the energies from the MM/PBSA per-residue decomposition for the THp peptide fragments (a and b) and for the 14-3-3γ monomers (c and d). Considering that the $\Delta G_{non\text{-}polar}$ values are small compared to the other energy terms in Table 3, and result from the contribution of many residues, it is fair to assume that they are negligible for individual residues (Fig. 3). The two analyses on the 14-3-3γ monomers (Fig. 3c and d) are in good agreement with each other and provide the same picture of the interaction with the THp peptide fragments, both in terms of identifying the main contributing residues and with regard to the energy values themselves. The few differences observed might be a consequence of the difference in fragment sequence coverage. Although the two simulated fragments are partially overlapping sequences from the same phosphorylated TH peptide, they still constitute two different peptides. Both THp-(14-26) and THp-(11-22) displayed negative $\Delta G'$ values in the MM/PBSA analysis (Table 3), implying that the enthalpy changes related to binding of the TH peptide fragments to 14-3-3γ contribute favorably to the free energy of binding. It is important to remember, though, that the entropy term is omitted from the analysis. As evidenced by the large and negative ΔE_{vdW} values (Table 3) and by the non-polar contributions in Fig. 3, van der Waals interactions contribute significantly to the favorable enthalpies of binding. However, the per-residue decomposition analyses also disclose that Arg132, Arg57 and Tyr133 play an important role as these residues make the most favorable contributions to the total binding enthalpy (Fig. 3c and d). These residues are conserved in the 14-3-3 protein family and are involved in phosphopeptide ligand binding [62,63]. Our results are thus consistent with a peptide-binding groove with partly hydrophobic and partly basic properties [23–25].

The occupancies for hydrogen bonds involving the three main contributors to a favorable enthalpy in Fig. 3 and the Ser19 phosphate oxygens agree with the crucial role of the phosphate group in binding the THp fragments to 14-3-3γ (Table 4). Hydrogen bond occupancy corresponds to the percentage of analyzed simulation time in which the relevant hydrogen bond existed. To distinguish the participating atoms from each other, we gave them different atom names in Table 4. Very stable interactions were maintained between the Ser19 phosphate in the TH

Table 2. Summary of the different simulation systems involving TH peptide variants

System	Peptide:protein	Number of POPS lipids	Number of sodium ions	Number of TIP3P waters	Simulation time (ns)
A	14-3-3γ dimer:THp fragments[a]	—	—	21,124	100
B	TH-(1-43)	—	—	3159	500
C	THp-(1-43)	—	—	2773	500
D	TH-(1-43)	128	128	13,290	500
E	THp-(1-43)	128	128	13,296	500

[a] THp-(14-26) and THp-(11-22), each bound to a 14-3-3γ monomer.

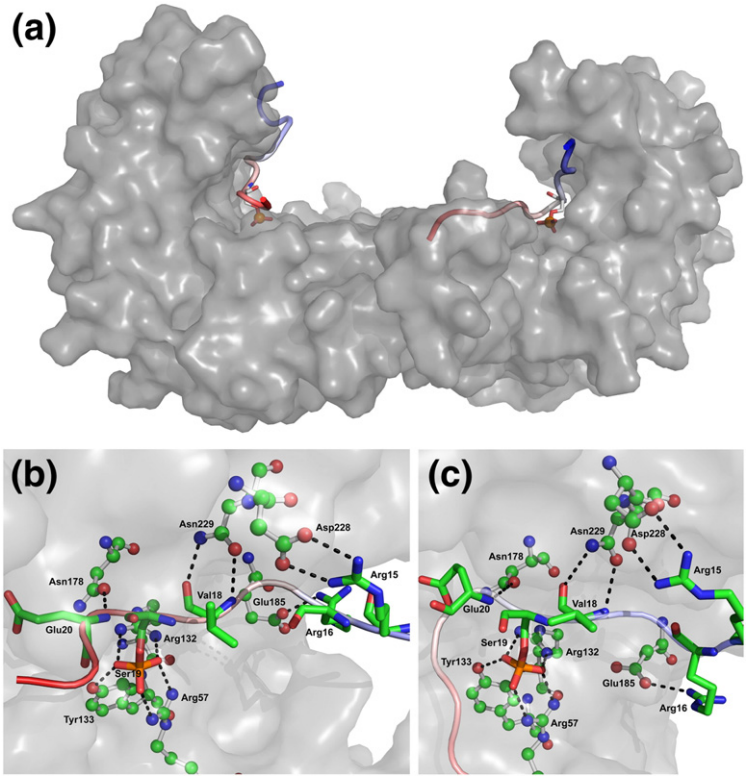

Fig. 2. Representative structure and interactions from the 14-3-3γ:THp peptide complex simulation. (a) The 14-3-3γ dimer as a gray surface with THp-(Ala11-Asp22) bound to the left monomer and THp-(Phe14-Ala26) bound to the right monomer. The peptides are colored as continuous gradients going from blue (N-terminus) to red (C-terminus). In addition, the Ser19 residue in each THp fragment is highlighted in the form of a stick model. (b and c) Shown are close-ups revealing the most important hydrogen bond interactions (broken lines) for THp-(Ala11-Asp22) (b) and THp-(Phe14-Ala26) (c) taking place in the structure of the complex (a). 14-3-3γ residues are shown as ball-and-stick representations and THp residues are shown as sticks. Water molecules have been removed for clarity.

fragments and Arg132, Arg57 and Tyr133, explaining the strong favorable contributions made by those 14-3-3γ residues in the energy decomposition analysis (Fig. 3). These results are in accordance with the fact that the Arg132-Arg57-Tyr133 triad corresponds to the conserved phosphopeptide binding motif in 14-3-3 proteins [23–25].

On the other hand, the sequence of the neighboring residues of Ser19 in TH does not comply with sequences considered to be optimal for 14-3-3 binding, that is, RSXpSXP (mode 1) and RX(Y/F)XpSXP (mode 2) [23,25]. It was therefore of interest to conduct a detailed analysis of the non-canonical intermolecular interactions involving THp residues in the vicinity of Ser19. The occupancies for hydrogen bonds formed during the last 50 ns of simulation between residues of 14-3-3γ and those surrounding Ser19 in both THp peptide fragments were calculated (Table 5). Considerable interaction was observed between the side chains of Asn229 and Asn178 in 14-3-3γ and the backbone of the pSer – 1 and the pSer + 1 residues, respectively (Table 5 and Fig. 2). These interactions agree with those previously reported for the corresponding residues in several 14-3-3 isoforms bound to mode 1 or mode 2 phosphopeptides [23,25]. TH has an alanine in the pSer – 2 position, as opposed to Ser (mode 1) or Tyr/Phe (mode 2). It is worth noting, though, that, despite the difference in residue size, the Ala17 side chain in both of our simulated peptide fragments was directed toward the same hydrophobic pocket in which the pSer – 2 Tyr resides in mode 2 phosphopeptide: 14-3-3ζ complexes [25]. The pSer – 4 Arg in mode 2 phosphopeptides complexed to 14-3-3ζ folds back into the phosphopeptide binding site and forms favorable salt bridges with the Ser19 phosphate and the Glu180 side chain (corresponds to Glu185 in γ) [25]. Instead, we see that Arg15 interacts favorably with Asp228 while Glu185 forms hydrogen bonds with Arg16, creating a well-packed, high-affinity complex.

The conformation of unbound TH-(1-43) and effect of phosphorylation at Ser19

In order to investigate the structural propensities of the TH N-terminal sequence in its unphosphorylated [TH-(1-43)] and phosphorylated [THp-(1-43)] states,

Table 3. Binding enthalpy from the simulated dimeric 14-3-3γ:THp peptide complex simulation decomposed into its component terms

Energy terms	Monomeric component[a]	
	THp-(Phe14-Ala26): 14-3-3γ	THp-(Ala11-Asp22): 14-3-3γ
ΔE_{vdW}	−69.5 ± 8.8	−49.8 ± 6.4
$\Delta E_{elec} + \Delta G_{PB}$	21.6 ± 10.6	17.7 ± 10.4
$\Delta G_{non\text{-}polar}$	−10.7 ± 0.9	−9.0 ± 0.5
$\Delta G'$	−58.6 ± 8.6	−41.1 ± 7.2

[a] The simulated dimeric 14-3-3γ:THp peptide complex was divided into its component 14-3-3γ monomer:peptide fragment pairs before both were subjected to MM/PBSA analysis.

we subjected the peptide sequences to MD simulation, using the configurations of the minimized structures as the starting structures for the simulations performed in water (Systems B and C in Table 2). Given in Fig. 4a are the *B*-factors for the α-carbon atoms in TH-(1-43) and THp-(1-43), computed from the last 100 ns of both the water and membrane simulations (Systems B–E in Table 2). Very high *B*-factors for most of the TH-(1-43) atoms imply that the unphosphorylated peptide was highly flexible in the aqueous simulation. Moreover, it can be inferred from the overall greater values in Fig. 4a that TH-(1-43) was considerably more flexible in water than THp-(1-43). The *B*-factor analysis is consistent with the propensity for formation of internal hydrogen bonds in the two peptides. As an example, only two residues (Arg16 and Glu20) in TH-(1-43) engaged in side chain–side chain hydrogen bond interactions with occupancies >25% in the last 100 ns of aqueous simulation. This reflects the high flexibility of the peptide, which precludes the visualization of a representative structure of TH-(1-43) from the

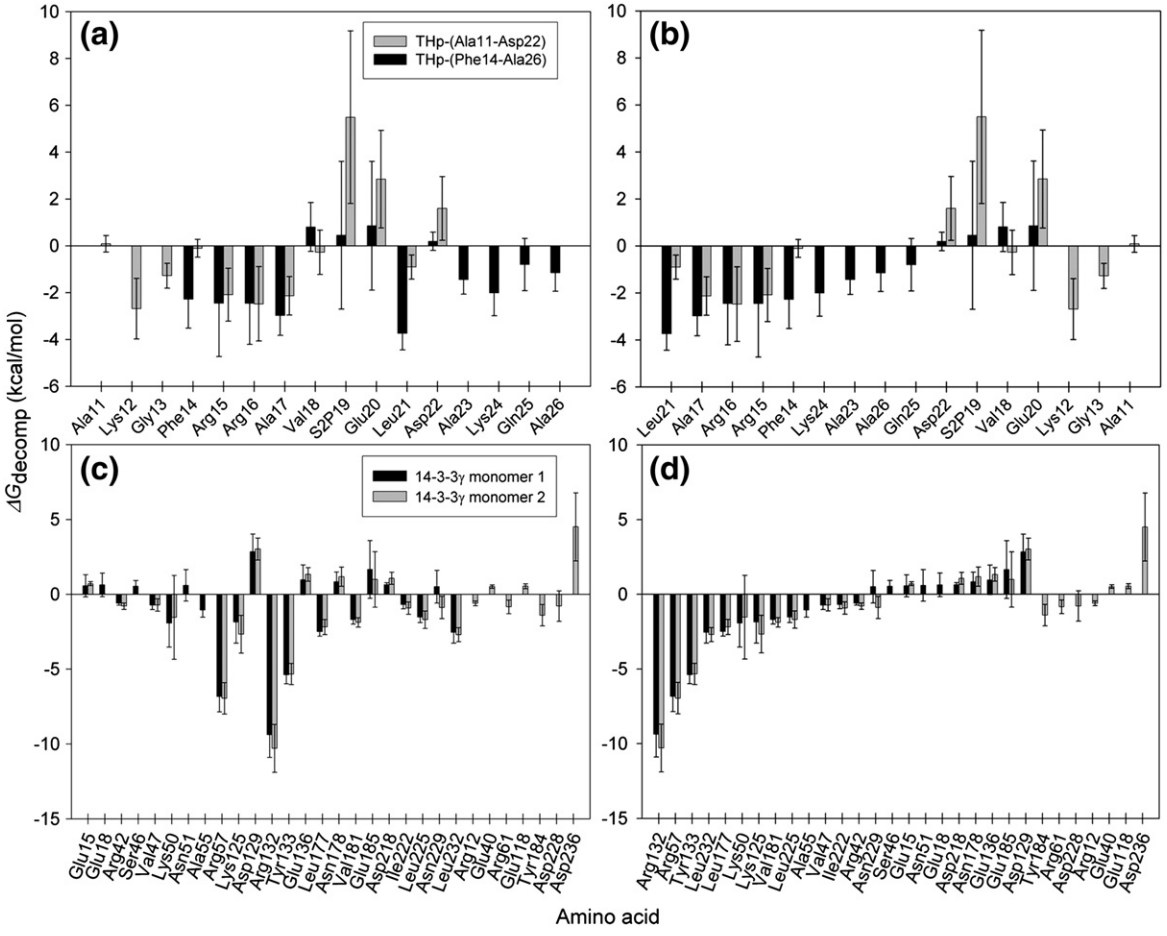

Fig. 3. MM/PBSA per-residue decomposition energies for the crystallographic 14-3-3γ:THp peptide complex after simulation. The calculations were performed for the two TH peptide fragments (a and b) and for the corresponding monomers of 14-3-3γ (c and d), using 1000 frames representing the last 50 ns of the crystallographic 14-3-3γ:THp peptide complex simulation (System A in Table 2). ΔG_{decomp} corresponds to the binding enthalpy [$\Delta G'$ in Eq. (4) and Table 3] minus the non-decomposable, but most likely negligible, non-polar contribution to the solvation energy [$\Delta G_{non\text{-}polar}$ in Eq. (4) and Table 3]. (a and c) Sorted by amino acid sequence. (b and d) Sorted in ascending order based on the decomposition energies for THp-(14-26) and 14-3-3γ monomer 1, respectively. In terms of 14-3-3γ, only the residues making contributions greater than ±0.5 kcal/mol are shown.

Table 4. Occupancies for hydrogen bond interactions between the three residues in 14-3-3γ that contributed most to the negative total enthalpic energy and the phosphate oxygens of Ser19 in the phosphorylated THp peptide fragments

14-3-3γ residue[a]	Ser19 oxygen[b]	Hydrogen bond occupancy (%)[c]	
		THp-(Phe14-Ala26)	THp-(Ala11-Asp22)
Arg132 (HH22)	O2P	100.0	93.0
Arg132 (HH12)	O1P	100.0	92.9
Arg132 (HH12)	O2P	40.7	44.1
Arg132 (HH22)	O1P	24.7	16.1
Arg57 (HH12)	O3P	100.0	89.0
Arg57 (HH22)	O1P	100.0	89.4
Arg57 (HH12)	O1P	61.3	62.7
Tyr133 (HH)	O2P	100.0	93.0

[a] Given in parentheses are hydrogens in the residues; HH12 and HH22 are amine hydrogens in the arginine side chain, while HH refers to the hydroxyl hydrogen in tyrosine.
[b] O1P, O2P and O3P correspond to the phosphate oxygens in THp-(Ser19).
[c] Percentage of the last 50 ns of 14-3-3γ:THp simulation time in which the interaction partners formed a hydrogen bond interaction (characterized by a distance of <3.5 Å between the non-hydrogen atoms and a donor–hydrogen–acceptor angle $>120°$).

simulation in water. Comparatively, quite a few stable side chain–side chain interactions involving several residues were formed in THp-(1-43), and a representative conformation from the aqueous simulation is presented in Fig. 4b. All these interactions involved arginines, and the phosphate at Ser19 participated in stable hydrogen bonding with the Arg37 side chain. This is in agreement with the *B*-factor analysis since the highlighted residues in Fig. 4b also gave the lowest *B*-factors in THp-(1-43) (Fig. 4a).

We also calculated the total number of intramolecular hydrogen bonds in each of the two peptides averaged over the last 100 ns of aqueous simulation, obtaining 24.0 ± 3.8 for TH-(1-43) and 37.3 ± 4.1 for THp-(1-43). In support of the *B*-factor analysis, it indicates that internal hydrogen bond interactions are much more prominent in the phosphorylated peptide, as revealed by the substantially higher bond count. Intrapeptide hydrogen bonds stabilize the structure. At the same time, the difference correlates well with the secondary structure content estimated for the two peptides (Table 6). For the aqueous simulations, more secondary structure is found in THp-(1-43). Furthermore, a count of the backbone–backbone NH–CO hydrogen bonds formed between amino acids separated by two, three or four residues provides values in accordance with the differences in flexibility and helix formation between the two peptides. Using a cutoff of 50% occupancy within the last 100 ns of simulation, we found the number of such interactions to be 12 in THp-(1-43) compared to 4 in TH-(1-43).

Together, these analyses suggest that phosphorylation of Ser19 induces a structuration resulting in a more stable, compact and less flexible peptide with more secondary structure content. However, these results do not seem to be supported by previous studies, including CD analysis, which indicated very similar structures for TH-(1-43) and THp-(1-43) in 20 mM citric acid–phosphate (pH 7.4), with a similar α-helical content of about 15–16% [22]. For some peptides, the CD spectra and estimated secondary structure content are also dependent on the ionic strength and type of buffer in the peptide solutions (see, e.g., Ref. [64,65]). We therefore performed CD analyses of the peptides at 2.5-fold higher concentration than in our previous study, both in water and

Table 5. Occupancies for hydrogen bond interactions between residues surrounding Ser19 in both phosphorylated TH peptide fragments and 14-3-3γ residues

THp residue[a]	14-3-3γ residue[a]	Hydrogen bond occupancy (%)[b]	
		THp-(Phe14-Ala26)	THp-(Ala11-Asp22)
Arg15 (HH12)	Asp228 (OD1)	33.4	70.6
Arg15 (HH12)	Asp228 (OD2)	32.4	55.4
Arg15 (HH22)	Asp228 (OD2)	29.3	74.4
Arg15 (HH22)	Asp228 (OD1)	28.7	66.2
Arg16 (HH21)	Glu185 (OE2)	29.6	49.6
Arg16 (HE)	Glu185 (OE1)	26.1	35.7
Val18 (H)	Asn229 (OD1)	95.7	71.8
Val18 (O)	Asn229 (HD21)	56.9	91.2
Glu20 (H)	Asn178 (OD1)	80.6	59.1

[a] Given in parentheses are names that were given to the different interacting atoms in the simulation: HH12, HH21, HH22 and HE are different guanidinium hydrogens in the arginine side chain; OD1/OD2 in aspartate and OE1/OE2 in glutamate are the side-chain carboxyl oxygens; HD21 and OD1 in asparagine denote one of the amine hydrogens and the carbonyl oxygen in the side chain; O and H refer to the backbone amide oxygen and amide hydrogen in the specified residue.
[b] Percentage of the last 50 ns of 14-3-3γ:THp simulation time in which the interaction partners formed a hydrogen bond interaction (characterized by a distance of <3.5 Å between the non-hydrogen atoms and a donor–hydrogen–acceptor angle $>120°$). Only interactions with occupancies above 25% in both monomer:peptide pairs are shown.

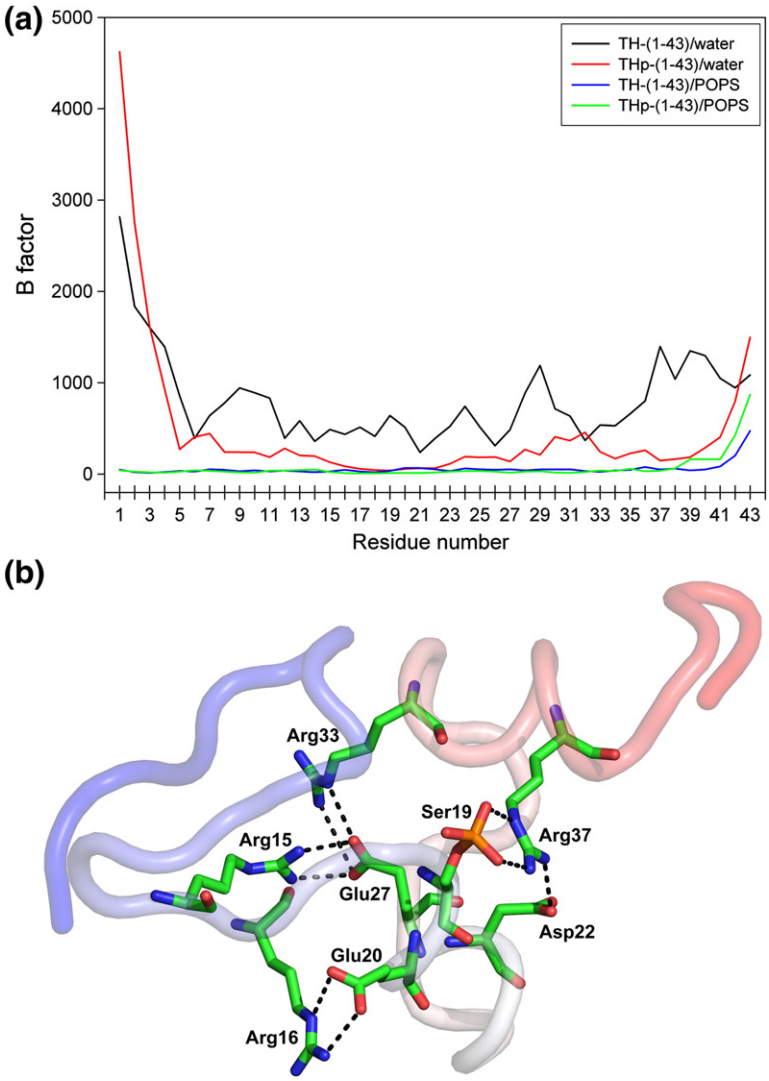

Fig. 4. *B*-factors for the α-carbons of the N-terminal fragments of TH and representative structure and interactions from the aqueous THp-(1-43) simulation. *B*-factors (a) were calculated from the aqueous simulations for TH-(1-43) (black line) and THp-(1-43) (red line) and from the peptide/membrane simulations for TH-(1-43) (blue line) and THp-(1-43) (green line) and are represented as a function of residue number. (b) Representative structure of THp-(1-43) that shows the intrapeptide side chain–side chain hydrogen bonds with occupancies >25% (broken lines) in the aqueous simulation. The peptide is colored as a continuous gradient going from blue (N-terminus) to red (C-terminus). The last 100 ns of each simulation was used for both analyses.

in 10 mM Hepes and 150 mM NaCl (pH 7.4). As previously described [22], we obtained very similar spectra for both peptides, which appear to adopt a higher structuration in water than in buffer, with a clearly higher negative molar ellipticity at 222 nm, corresponding to higher helical content (Fig. S1, in

Table 6. Content of secondary structure in the unphosphorylated TH-(1-43) and Ser19-phosphorylated THp-(1-43) peptides, estimated from the simulations both in water and with the POPS bilayer

Interaction partner	α-Helix (%)[a]		β-Sheet (%)[a]		Turn (%)[a]	
	TH-(1-43)	THp-(1-43)	TH-(1-43)	THp-(1-43)	TH-(1-43)	THp-(1-43)
POPS bilayer	11.7 ± 5.7	8.0 ± 5.3	4.2 ± 1.2	0.3 ± 1.1	26.8 ± 6.0	22.0 ± 6.3
Water	8.9 ± 5.5	23.7 ± 5.8	0.2 ± 1.0	1.8 ± 2.2	19.1 ± 6.8	21.8 ± 5.9

[a] The proportion of the peptide adopting the specified type of secondary structure, averaged over the last 100 ns of simulation.

supplementary data). At the same time, the estimated secondary structure contents were only slightly higher in water than in buffer. For instance, the α-helical and random-coil contents estimated for THp-(1-43) by CDNN [35] were about 15% and 49% in water *versus* 13% and 51% in buffer, respectively. In fact, these values were not so different from the estimates for TH-(1-43). Similar values were obtained with other programs (data not shown), and significant differences were not proven for the two peptides. For loosely folded peptides and proteins, many possible conformations exist, as is expected from the Boltzmann distribution. CD will detect an average of these distributions across the sample volume and time resolution of the experiment, while MD simulations follow one of many possibilities that are close in energy and conformational space, probably catching the dissimilarity of TH-(1-43) and THp-(1-43) with respect to conformational propensity.

A structuration upon phosphorylation is in agreement with structural analyses on the effect of phosphorylation of phenylalanine hydroxylase at Ser16, which was found to cause a localized conformational change in the N-terminal segment [66]. The region surrounding Ser16 adopted a bent and thereby more compact configuration, a reorientation postulated to primarily result from favorable electrostatic interaction between the introduced phosphate group and Arg13. Phosphorylation was also accompanied by an increase in α-helix content. Moreover, Stultz *et al.* deduced from fluorescence resonance energy transfer measurements and MD simulations that the peptide TH-(24-33) becomes more compact upon phosphorylation of Ser31 due to formation of a salt bridge between the phosphate and Arg33 [67].

The binding of TH-(1-43) and THp-(1-43) to the POPS membrane

Previous studies have shown that full-length TH [19] and both TH-(1-43) and THp-(1-43) [22] interact selectively with membranes of mixtures of zwitterionic and negatively charged lipids. The unphosphorylated peptide showed 5- to 8-fold higher affinity than the phosphorylated peptide [22], as measured by the $S_{0.5}$ (concentration of peptide for half-maximal binding obtained from binding isotherms). In the present study and in order to investigate the conformational determinants for the peptide:membrane interaction by MD simulations, we selected a bilayer made of palmitoyl-oleoyl phosphatidylserine (POPS) (see Materials and Methods). Membrane binding of TH-(1-43) and THp-(1-43) was previously tested [22] using liposomes made of phospholipid mixtures, which can favor protein interaction relative to bilayers composed of a unique negatively charged phospholipid [68]. In this study, we therefore confirmed by SPR analyses that the peptides also interacted with liposomes made of pure POPS. The peptides showed only slight binding to liposomes made of phosphatidylcholine (PC), and the response units (RU) with these liposomes (at the reference channel) were subtracted from the RU in the channel with POPS to compensate for non-specific binding. The sensorgrams for TH-(1-43) binding to POPS liposomes at increasing peptide concentration are shown in Fig. 5a. The binding was concentration dependent (Fig. 5b), and although $S_{0.5}$ was found to be similar for both peptides [53.3 ± 9.2 μM and 48.2 ± 7.4 μM for TH-(1-43) and THp-(1-43), respectively], the unphosphorylated peptide certainly showed a larger extent of membrane binding.

We then performed simulations of TH-(1-43) and THp-(1-43) with the POPS bilayer model (Systems D and E in Table 2). Representative structures from these simulations, together with close-ups of the most important hydrogen bond interactions in each case, are depicted in Fig. 6a–d. As determined by the *B*-factors for the α-carbon atoms, both peptides were much more structurally stable and a lot less flexible in the presence of the lipid bilayer than was the case in the aqueous simulations (Fig. 4a). The membrane-interacting peptides showed rather similar *B*-factor profiles apart from the last couple of residues in the C-terminal region, where the THp-(1-43) residues proved more flexible. Contrary to the situation in water, TH-(1-43) shows a trend toward higher content than THp-(1-43) of all three types of secondary structure in the membrane simulations (Table 6). However, the estimations are hampered by large standard deviations. The findings appear to be in accordance with experimental results obtained by CD for the interaction of the peptides with negatively charged phospholipid bicelles and with the increased propensity of TH-(1-43) for acquiring secondary structure in response to increasing concentrations of trifluoroethanol used as a membrane-mimicking solvent [22]. Furthermore, the higher stabilization of the membrane-bound peptides with respect to their conformations in water is also in agreement with earlier results showing that TH is stabilized against thermal denaturation in the membrane-bound state [19]. Here, we performed CD analyses of the peptides in the presence of liposomes made of POPS. Bicelles are superior to liposomes with regard to use in spectroscopic techniques due to their smaller volume, which causes less noise in CD measurements [22]. However, bicelles cannot be prepared with a sole composition of phospholipid, and CD spectra could not be taken in the presence of high liposome content. With a liposome content corresponding to 0.6 mM phospholipid, similar CD spectra were obtained for both peptides, with increased ellipticity at 222 nm compared to the spectra obtained without liposomes (Fig. 5c). This may reflect their stabilization at the membrane. The liposomes are not stable in water and measurements can only be performed in buffer.

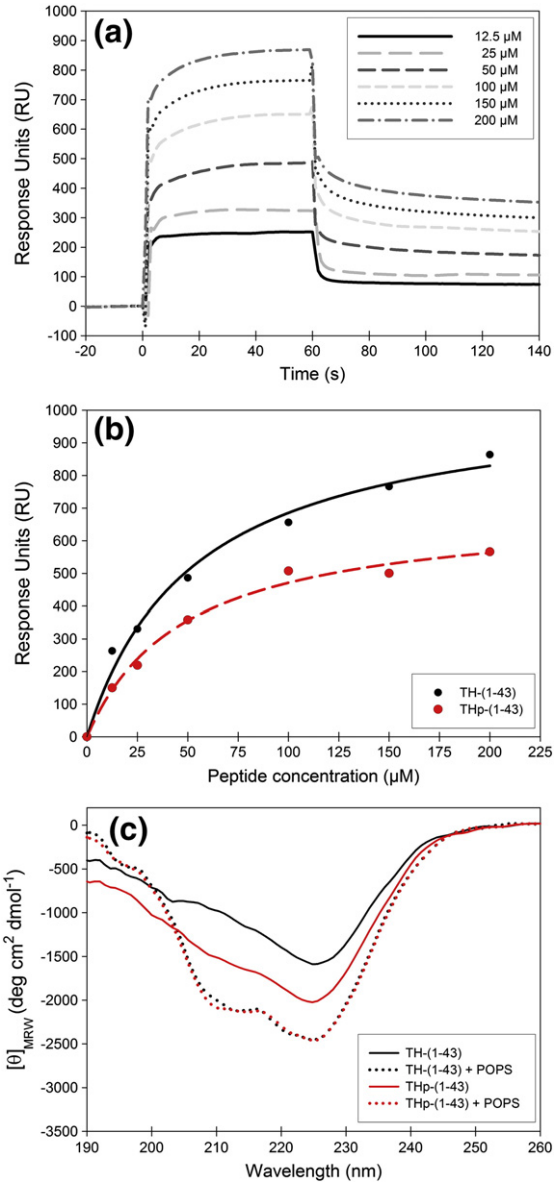

Fig. 5. Binding of TH-(1-43) and THp-(1-43) to POPS liposomes by SPR and CD. (a) Representative sensorgrams for the interaction of TH-(1-43) with POPS liposomes on a L1 sensor chip at increasing concentrations of peptide. (b) Peptide concentration dependency of TH-(1-43) (black) and THp-(1-43) (red) when bound to POPS liposomes. RU were measured as a function of peptide concentration. $S_{0.5}$ values were extracted from the hyperbolic, single-rectangular, two-parameter curve fitting and resulted in $S_{0.5}$ of 53.3 ± 9.2 μM and 48.2 ± 7.4 μM for TH-(1-43) and THp-(1-43), respectively. (c) Far-UV CD spectra of 40 μM TH-(1-43) (black lines) or THp-(1-43) (red lines) without (continuous lines) or with (dotted lines) POPS liposomes (0.6 mM phospholipid). Samples were prepared in 10 mM Na–Hepes and 150 mM NaCl (pH 7.4), and spectra were recorded at 25 °C.

To get a more detailed picture of the peptide: membrane interactions, we carried out MM/PBSA decomposition analyses. The total enthalpic energy changes ($\Delta G'$) for each system and the contributions from the energy terms in Eq. (4) are presented in Table 7. In addition, the $\Delta\Delta$ values for each term, calculated as the energy differences between the TH-(1-43)/POPS and the THp-(1-43)/POPS systems, are given. Figure 7 shows the decomposed energies of the two peptides from the MM/PBSA analysis on a per-residue basis. As in the analysis of the 14-3-3ζ:THp simulations (Fig. 3), ΔG_{decomp} refers to binding enthalpy ($\Delta G'$), but without inclusion of the non-decomposable $\Delta G_{non\text{-}polar}$ term. Favorable binding enthalpies were observed for both peptides upon interaction with the POPS bilayer model, as shown by the negative $\Delta G'$ values in Table 7. However, the binding enthalpy is approximately 40 kcal/mol smaller for the THp-(1-43)/POPS system, indicating that binding of TH-(1-43) to the POPS membrane is much more enthalpically favorable than is the case for the Ser19-phosphorylated counterpart. Differences between the two peptides with regard to van der Waals interactions (ΔE_{vdW}) and non-polar solvation energy ($\Delta G_{non\text{-}polar}$) are modest. Most of the difference in the overall binding enthalpy arises from the polar terms ($\Delta E_{elec} + \Delta G_{PB}$). In contrast to the TH-(1-43)/POPS system, the polar terms involved in THp-(1-43)/POPS interaction contribute unfavorably to the binding enthalpy. The phosphorylated Ser19 residue accounts for nearly the whole deviation in decomposition energies for the two peptides (Fig. 7). Excluding Ser19, only small differences between the peptides are seen in the per-residue decomposition energies. Accordingly, it seems that the introduction of the phosphate group causes repulsion between the peptide and the membrane. Not surprisingly, the positively charged arginines and lysines were the main contributors to the favorable enthalpy of binding to the POPS membrane observed for both peptides, with Arg15 and Arg16 being the most important (Figs. 6 and 7). Negatively charged aspartates and glutamates, together with the phosphorylated Ser19 in THp-(1-43), contributed unfavorably to the total binding enthalpy (Fig. 7), implying that the decomposition results are reasonable from an electrostatic point of view.

The importance of Arg15 and Arg16 in the interaction with the membrane becomes more apparent in Fig. 6b and d, where extensive interaction between POPS lipids and the two arginines in both peptides is shown. However, Arg16 in THp-(1-43) is partly diverted away from the bilayer through favorable interaction with the Ser19 phosphate (Fig. 6d) rather than fulfilling its hydrogen bonding potential by binding to the membrane only (Fig. 6b). This intramolecular interaction might also contribute to the observed difference in $\Delta G'$ between TH-(1-43)/POPS and THp-(1-43)/POPS (Table 7).

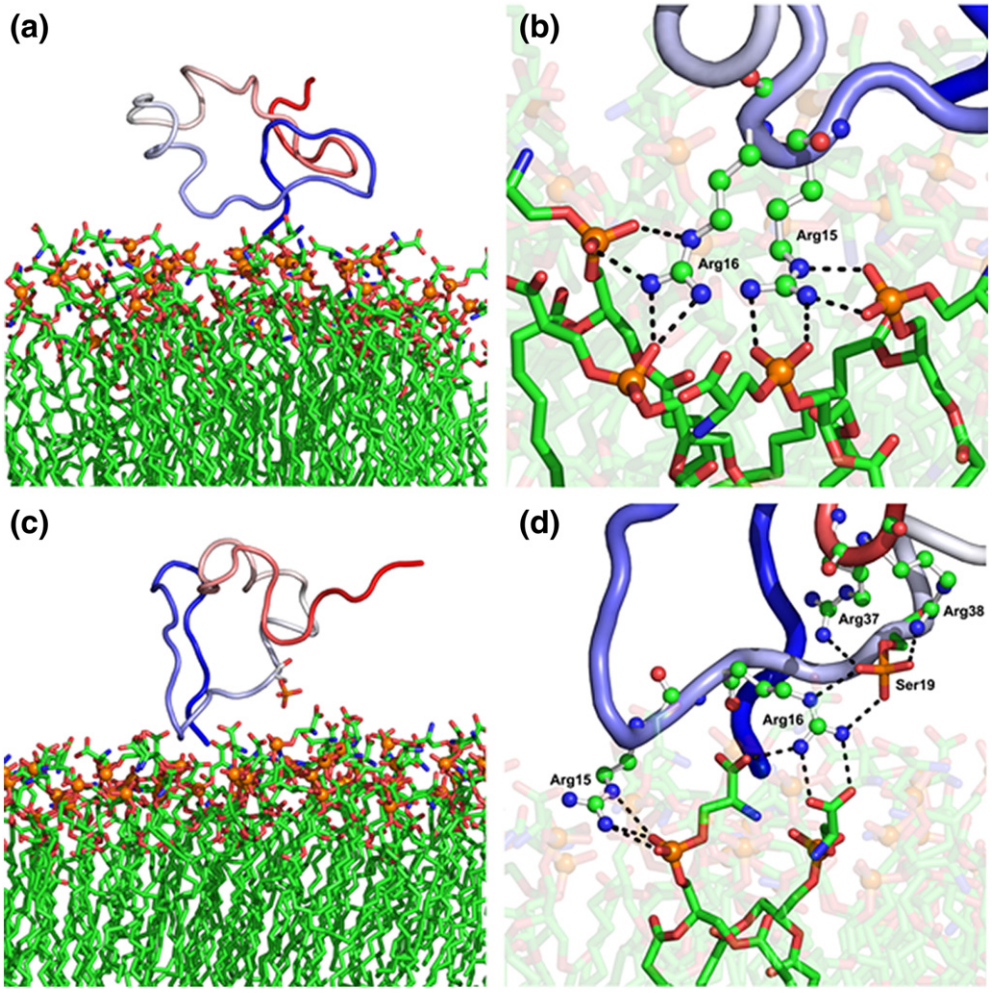

Fig. 6. Representative structures and interactions from the peptide/membrane simulations. TH-(1-43)/POPS is presented in (a) and (b), and THp-(1-43)/POPS is presented in (c) and (d). (a and c) The peptide—colored as a continuous gradient going from blue (N-terminus) to red (C-terminus)—together with most of the peptide-interacting leaflet of the POPS bilayer, the orange spheres representing the head group phosphorus atoms. (b and d) Close-ups of the most important hydrogen bond interactions (broken lines) in each case, where the relevant TH residues are displayed as ball-and-stick models and the POPS lipids are displayed as sticks. Water and ions have been removed for clarity.

Table 7. Binding enthalpy for the peptide/membrane simulations decomposed into its component terms

Energy terms[a]	System[b]		Energy difference (kcal/mol)
	TH-(1-43)/POPS	THp-(1-43)/POPS	
ΔE_{vdW}	−26.1 ± 5.5	−21.8 ± 7.4	−4.3
$\Delta E_{elec} + \Delta G_{PB}$	−21.8 ± 11.7	12.6 ± 13.8	−34.4
$\Delta G_{non\text{-}polar}$	−5.2 ± 0.6	−4.3 ± 0.9	−0.9
$\Delta G'$	−53.1 ± 10.8	−13.5 ± 9.8	−39.6

[a] $\Delta G'$ refers to the change in total enthalpy as given in Eq. (4).
[b] The peptide-interacting leaflet of the POPS bilayer constituted the receptor in these calculations.

Structural comparison of the TH N-terminal peptides in different states

We further measured the distances between the terminal α-carbons of each peptide fragment in the 14-3-3γ dimer:THp fragment complex (System A; Table 2) as a function of simulation time and averaged over the last 50 ns. The resulting values were compared with the distances between the corresponding α-carbons averaged over the last 100 ns of both the aqueous and membrane-containing simulations of THp-(1-43) and TH-(1-43) (Systems B–E in Table 2) (Table 8). These estimations provide a crude measurement of how extended the peptides were in each state. The distance between the α-carbons of Phe14 and Ala26 was 8 Å greater when bound to 14-3-3γ than in water. Following the same trend, the separation

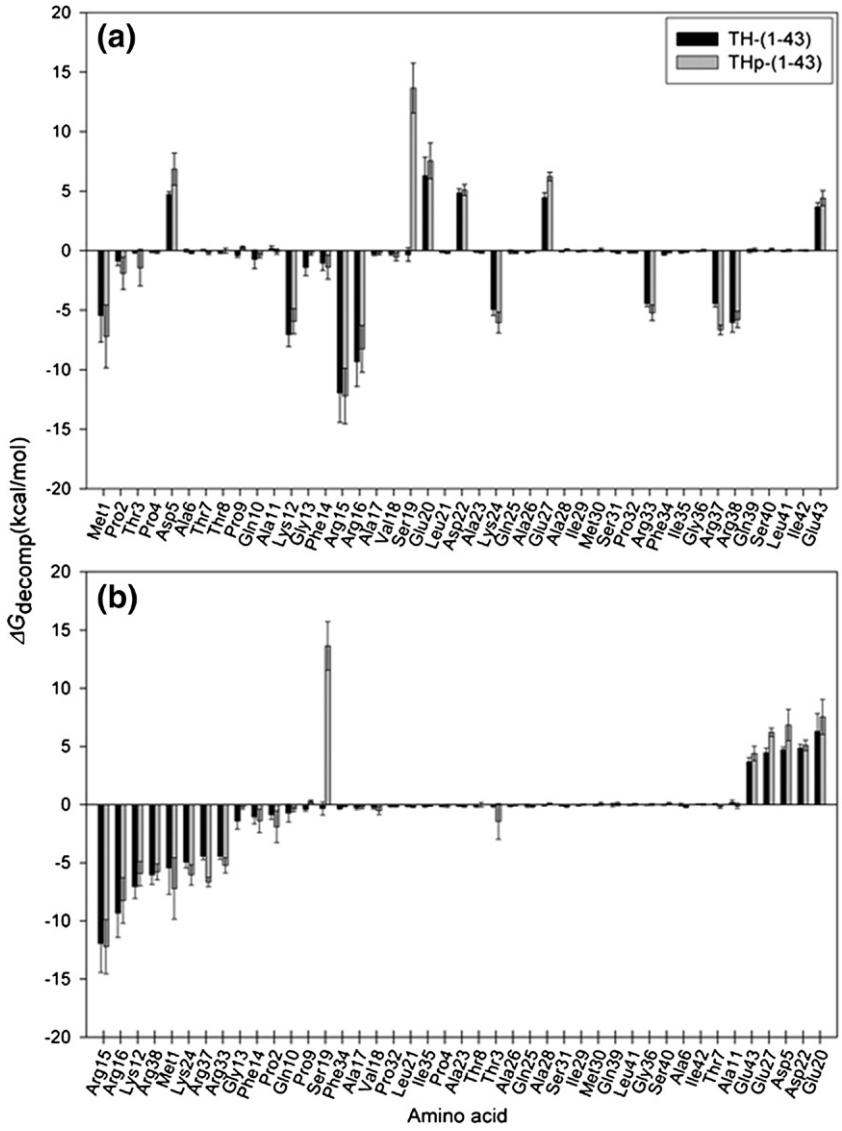

Fig. 7. MM/PBSA per-residue decomposition energies for TH-(1-43) and THp-(1-43) from the peptide/membrane simulations. The energies are computed using 1000 frames extracted from the last 100 ns of each peptide/membrane simulation (Systems D and E in Table 2). $\Delta G_{decomp} = \Delta G' - \Delta G_{non\text{-}polar}$. The black bars represent the energies derived for each residue in TH-(1-43), and the gray bars are the THp-(1-43) equivalents. (a) Sorted by amino acid sequence; (b) sorted in ascending order according to the TH-(1-43) decomposition energies.

between the Ala11 and Asp22 α-carbons was 13.1 Å greater when bound to 14-3-3γ than in water. In conclusion, this indicates that the region surrounding the Ser19 phosphate group in THp-(1-43) stretches out and accommodates a more extended conformation upon shifting from "free in solution" to the 14-3-3γ-bound state. The membrane-interacting version of the phosphorylated TH peptide gives distances that are intermediate compared to the 14-3-3γ-bound and solvated conformations. Positively charged residues in THp-(1-43) that, in water, are available for intramolecular interactions with negatively charged residues (Fig. 4b) interact favorably with the POPS bilayer (Figs. 6d and 7). With regard to TH-(1-43), the results are ambiguous and appear to be more random (Table 8). Also, the standard deviations related to the distances derived from the aqueous simulation are three times higher than for THp-(1-43), in line with the greater flexibility of the unphosphorylated peptide discussed earlier (Fig. 4a). These observations suggest

Table 8. Comparison of the distances between the terminal amino acids of the THp-(14-26) and THp-(11-22) fragments from the 14-3-3γ:THp simulation and the corresponding distances taken from the simulations of THp-(1-43) and TH-(1-43) in water and in the presence of the POPS bilayer

System	Distance (Å)	
	Phe14-Ala26	Ala11-Asp22
THp fragments (in the 14-3-3γ:THp complex)[a]	22.9 ± 2.1	26.9 ± 1.6
THp-(1-43)/water[b]	14.9 ± 0.9	13.8 ± 1.2
TH-(1-43)/water[b]	12.3 ± 2.7	18.9 ± 3.6
THp-(1-43)/POPS[b]	20.9 ± 0.8	15.3 ± 0.3
TH-(1-43)/POPS[b]	9.8 ± 0.6	21.3 ± 0.8

[a] Averaged over the last 50 ns of simulation.
[b] Averaged over the last 100 ns of simulation.

that the conformational sampling of the region around Ser19 is less dependent on the Ser19 residue than is the case in THp-(1-43).

Finally, we consider it probable that the binding mode displayed by the truncated THp-(1-43) peptide in its interaction with 14-3-3γ is the same as for this sequence in full-length TH. There is no structural information available for the 1-43 N-terminal segment in TH, which is an extension of the regulatory ACT domain equivalent to the extended N-terminus in TPH2 [29,30]. This N-terminal segment is associated with increased instability of TPH2 compared to TPH1, and phosphorylation of Ser19, which is also the determinant for binding to 14-3-3 in TPH2, increases its intracellular stability [29,69]. Furthermore, the N-terminal sequences in TH and TPH2 are predicted to be highly disordered using PONDR-FIT and DisProt [70,71]. Intrinsically disordered segments are most likely separated from the rest of the folded cores of the proteins but become structured by posttranslational modification and/or binding to a partner [72]. Consequently, it is highly probable that the rearrangements observed in the TH peptides upon phosphorylation and further by binding to 14-3-3 reflect the changes to the segment when connected to the enzyme. Nevertheless, other regions of TH might interact with 14-3-3 at areas remote from the phosphopeptide binding site, as observed for serotonin *N*-acetyltransferase bound to 14-3-3ζ [73].

Conclusions

As expected, the crystal structure of phosphorylated TH fragments complexed to 14-3-3γ, complemented by MD simulations and subsequent MM/PBSA analysis, indicates that the phosphate at Ser19 forms strong and stable interactions with the conserved phosphopeptide binding motif of 14-3-3γ. The region surrounding Ser19 adopted a more extended conformation when bound to 14-3-3γ than was the case in water and established similar interactions with the protein as found for other peptides with canonical mode 1 and mode 2 14-3-3 binding motifs. Our aqueous simulations suggest that phosphorylation of Ser19 induces a localized conformational change in the N-terminal segment of TH, resulting in a more compact and rigid configuration and an apparent increase in α-helix content. Both TH-(1-43) and THp-(1-43) bind to anionic POPS membranes, as indicated by SPR experiments and favorable binding enthalpies calculated for the initial stage of the peptide:membrane interactions using MM/PBSA. Binding seems to be mediated mainly by positively charged arginines and lysines. Electrostatic repulsion between the Ser19 phosphate and the negatively charged serine lipid head groups of the membrane gives a less favorable enthalpy of binding for THp-(1-43). Interaction with the POPS bilayer model appears to stabilize the structure of both peptides, notably TH-(1-43). Our results provide further insights on the conformational versatility of the N-terminal region (residues 1–43) of TH and on the influence of phosphorylation at Ser19 as a posttranslational modification that regulates the interaction of the enzyme with 14-3-3 and membranes, with concomitant changes in function and localization.

Materials and methods

Peptides and phospholipids

The peptides TH-(1-43) (MPTPDATTPQAKGFRRAV SELDAKQAEAIMSPRFIGRRQSLIE) and THp-(1-43) (MPTPDATTPQAKGFRRAVS(PO_3)^2-ELDAK QAEAIMSPRFIGRRQSLIE) were synthesized by CPC Scientific (San Jose, CA) at approximately 90% purity, as seen by mass spectroscopy, and used without further purification. PC from egg yolk lecithin (99% PC) and POPS were purchased from Avanti Polar Lipids, Inc.

Expression and purification of 14-3-3γ

Human 14-3-3γ was expressed using pGEX-expression vector in BL-21-CodonPlus® as glutathione *S*-transferase fusion proteins and was further purified on glutathione-Sepharose 4B (GE Healthcare) essentially as reported [22]. The fusion protein was cleaved by thrombin (4 U/ml) while attached to the column, at 4 °C for 1 h. The dimeric 14-3-3γ protein (about 56-kDa dimer) was further purified by gel filtration in HiLoad 16/60 Superdex 200 (Amersham Biosciences) in 50 mM sodium phosphate, 150 mM NaCl (pH 7.4), 1 mM dithiothreitol and 1 mM ethylenediaminetetraacetic acid and was further exchanged to 10 mM Tris and 200 mM NaCl (pH 8) (crystallization buffer, see below).

Crystallization and X-ray structure determination

The purified 14-3-3γ protein was concentrated up to 30 mg/ml (approximately 1.07 mM subunit) using Amicon® Ultra centrifugal filter units (molecular mass cutoff of 30 kDa)

(Millipore), and the synthetic THp-(1-43) peptide was prepared in 10 mM Tris and 200 mM NaCl (pH 8) to a concentration of 20 mg/ml (approximately 4 mM). 14-3-3ζ and THp-(1-43) were mixed at a molar ratio of 1:3 [14-3-3ζ:THp-(1-43) complex] to a concentration of 0.6 mM 14-3-3ζ subunit. After mixing and incubating on ice for 30 min, we ultracentrifuged the sample at approximately 200,000*g* for 10 min. The supernatant was dispensed in a clean tube and used for crystallization.

Crystals were grown by sitting-drop vapor diffusion using 96-well plates (Innovaplate SD-2; Innovadyne Technologies, Inc.) with the help of a dispensing robot (Innovadyne Screenmaker; Innovadyne Technologies, Inc.) and incubated at 10 °C. The 14-3-3ζ:THp-(1-43) complex was mixed in a 1:1 ratio with buffer containing 0.1 M K thiocyanate, with 30% polyethylene glycol 2000 monomethyl ether as precipitant. Small rectangular crystals (~60 μm × 40 μm × 20 μm) grew after 7 days, and they were harvested with a nylon cryoloop and soaked briefly in a solution consisting of 25% glycerol added to the crystallization buffer. The crystals were subsequently frozen directly into liquid nitrogen. X-ray diffraction data were collected at 100 K at the GM/CA-CAT beamline of the Advanced Photon Source (at Argonne) by using a 10-μm beam collimator. Data processing was performed by using the XDS software package [32]; the structure was solved using the dimeric 14-3-3ζ (PDB code 2B05) as a model for molecular replacement and refined with the programs Coot [33] and Refmac 5 from the CCP4 program suite [34].

Preparation of liposomes

Liposomes were prepared as large unilamellar vesicles, made of either PC or POPS as described previously [22]. Briefly, the chloroform-dissolved phospholipids were dried under nitrogen stream and subjected to vacuum for 2 h. The lipids were resuspended in 10 mM Na–Hepes and 150 mM NaCl (pH 7.4) and were left in an incubator overnight in the dark at 37 °C and 150 rpm. The hydrated phospholipid solutions were then frozen and thawed seven times, followed by extrusion (11 times) with the Avanti Mini-Extruder using a membrane of 0.1 μm pore size. The hydrodynamic diameter was measured by dynamic light scattering using a Zetasizer Nano-Instrument (Malvern) and was estimated to be 92.4 ± 0.6 and 115.4 ± 2.5 nm for liposomes made of PC and POPS, respectively.

Surface plasmon resonance

SPR analyses to monitor the interaction of TH-(1-43) and THp-(1-43) with liposomes composed of either PC or POPS were carried out using the Biacore 3000 biosensor (Biacore AB) and an L1 sensor chip at 25 °C. The conditions for deposition of the liposomes, application of the peptides to the captured liposomes and regeneration of the sensor chip surface were performed essentially as reported [22]. The values for non-specific binding measured in the reference cell (with liposomes consisting of PC) were subtracted. The BIA evaluation program version 3.2 (Biacore AB) was used for analysis of the sensorgrams. The binding isotherms for maximal RU *versus* concentration of peptide were found to be hyperbolic and were processed by nonlinear least-squares analysis. The concentration of peptide providing half-maximal binding ($S_{0.5}$) is thus a measure of the inverse of the apparent association or partition constant [$1/K_a$(app)]. The $S_{0.5}$ values provide comparative and operational measurements of affinity.

Circular dichroism

CD experiments were performed in the far-UV spectral range (180–260 nm) with a Jasco J-810 spectropolarimeter equipped with a Peltier element for temperature control, at 25 °C, using a data pitch of 0.1 nm, a bandwidth of 2 nm and a scan speed of 50 nm/min. Sample solutions were loaded into a 1-mm-quartz cuvette (Hellma), and CD spectra of TH-(1-43) and THp-(1-43) (both 50 μM) either in water or in 10 mM Na–Hepes and 150 mM NaCl (pH 7.4) were acquired. Spectra in the presence of liposomes made of POPS (0.6 mM liposome phospholipid) were taken in the same buffer with 40 μM peptide. Baseline spectra of buffer or liposomes without peptide were obtained and subtracted using the software provided by the instrument manufacturers, and data were smoothened using running average with a sampling proportion of 0.05. The mean residue ellipticity was determined using the formula $[\theta]_{MRW} = MRW \times \theta/(10 \times c \times l)$, where MRW is the mean residue weight (g/mol), θ is the ellipticity (°), 10 is a scaling factor, c is the protein concentration (g/ml) and l is the path length of the cuvette (cm). MRW is calculated from $MRW = M/(N - 1)$, where M is the molecular mass (g/mol) and N is the number of amino acids in the chain. Three parallels were averaged after subtraction, calculation of mean residue ellipticity and estimation of secondary structure by using the CDNN software [35].

MD simulations

14-3-3ζ with bound THp-(1-43) peptide

MD simulation was initiated using coordinates obtained from the three-dimensional X-ray structure including data up to 3.1 Å resolution. The final model of the 14-3-3ζ:THp-(1-43) complex included residues Phe14-Ala26/Ala11-Asp22 of the THp fragment (System A in Table 2), and the model was built as follows: two 14-3-3ζ dimers with THp fragments bound to each of the monomers were aligned using Accelrys Discovery Studio [36] and one of them subsequently deleted due to a very high degree of similarity between the two dimer conformations. The longest peptide fragments in the alignment were kept, and overlapping residues were removed to give a single peptide bound to each monomer. These peptide fragments were included in the simulation structure and capped with ACE and NME groups, as is standard in AMBER. In consequence, the system consisted of a 14-3-3ζ dimer with a 13-residue fragment (Phe14-Ala26) and a 12-residue fragment (Ala11-Asp22) bound to each monomer, respectively (Table 2). The complex was solvated by an octahedral-shaped water box and subjected to the following minimization and simulation steps: (i) minimization for 10,000 steps, (ii) 5 ps gradual heating from 0 to 100 K (NVT) with restraints on 14-3-3ζ and peptide fragments, (iii) 100 ps gradual heating from 100 to 300 K

(NPT) with restraints on 14-3-3γ and peptide fragments, (iv) 100 ps equilibration (NPT) with restraints on peptide fragments, (v) 1 ns equilibration (NPT) without restraints and (vi) 100 ns simulation (NPT) without restraints.

Pure POPS membrane

The start configuration for the simulation of the pure POPS bilayer was the equilibrated end structure from an MD study by Mukhopadhyay *et al.* [37], obtained as a PDB file by correspondence with co-author Luca Monticelli. The system had been simulated for 40 ns and consisted of a united atom representation of 128 POPS molecules, 128 neutralizing sodium ions and 5391 water molecules. Following the addition of aliphatic hydrogens to obtain an all-atom model, we used six of the POPS conformations for charge derivation in Gaussian 03 [38]. The resulting electrostatic potential surfaces were fitted to atomic point charges by virtue of a RESP procedure [39], and the average charges calculated from the six conformations were applied in all the simulations involving POPS. Antechamber [40] assigned GAFF atom types [41] to the membrane lipids. Subsequent minimization and equilibration of the pure membrane system were performed as previously described [42]. The area per lipid was kept constant at 53.54 $Å^2$, close to the average value of 55 ± 1 $Å^2$ derived by Mukhopadhyay *et al.* [37].

TH peptides in water and with the POPS membrane

The peptides TH-(1-43) and THp-(1-43) were built as random coils with the protein builder in Accelrys Discovery Studio [36] and simulated for 100 ns in explicit octahedral-shaped water boxes. The final peptide conformations from these simulations were subjected to another 500 ns of aqueous simulation at 300 K using the NPT ensemble (Systems B and C in Table 2), and the same peptide conformations were inserted into the aqueous phase of the pure POPS bilayer system (see above). The water phase had to be extended through addition of extra water molecules in PACKMOL in order to fully accommodate the peptides [43]. The resulting membrane/peptide simulation systems are described in Table 2 (Systems D and E). Both were subjected to the same minimization and simulation procedure: (i) minimization for 10,000 steps without restraints, (ii) 5 ps gradual heating from 0 to 100 K (NVT) with restraints on membrane and peptide; (iii) 100 ps gradual heating from 100 to 300 K (NPT) with restraints on membrane and peptide; (iv) 1 ns equilibration of water (NPT) with restraints on membrane and peptide and (v) 500 ns simulation at constant volume (NVT) without restraints.

All simulations were performed with AMBER12 [44]. Periodic boundary conditions were applied for all systems and enabled the particle mesh Ewald method [45,46] to sum the electrostatic interactions by fourth-order B-spline interpolation and with a grid spacing of <1 Å. van der Waals forces were truncated by a 10-Å cutoff. By means of the SHAKE algorithm [47], the lengths of the covalent bonds involving hydrogen were constrained, which allowed for time steps of 2 fs. Pressure was regulated anisotropically for the constant pressure portion of the membrane simulations, while isotropic scaling was applied for the peptides in pure water and for the simulation of the 14-3-3γ:THp peptide complex. In both cases, the target pressure was maintained at 1 bar. The Langevin thermostat [48] controlled the temperature. Force constants for the positional restraints referred to in previous sections differed depending on the type of calculation, with 500 kcal/mol $Å^2$ used for minimization and 10 kcal/mol $Å^2$ applied in the relevant simulation steps. All the peptides and 14-3-3γ were modeled by the ff99SB force field [49], apart from the phosphoserine group in THp-(1-43) and in the THp-(1-43) fragments in the complex, which required specific parameters developed by Homeyer *et al.* [50]. Water molecules were described by the TIP3P model [51].

Trajectory analysis

Several types of MD trajectory analysis were performed, including *B*-factor, hydrogen bonding and secondary structure analysis. A brief description of each of them is provided in the following.

In the context of MD simulations, *B*-factors are defined to be directly proportional to the squared root-mean-square fluctuations (RMSF) of the atomic positions:

$$B\text{-factor} = \frac{8\pi^2}{3}\mathrm{RMSF}^2 \quad (1)$$

As such, they represent how much atoms move in the course of the simulation and thereby give a measure of flexibility. *B*-factors were derived according to Eq. (1) using ptraj [44].

Hydrogen bond counts and occupancies were calculated by the cpptraj facility [44]. For an interaction to be classified as a hydrogen bond, the distance between the non-hydrogen atoms had to be <3.5 Å and the donor–hydrogen–acceptor angle had to be $>20°$.

Secondary structure content was estimated by DSSP [52] as implemented in the ptraj secstruct program [44]. The proportions of each peptide that adopted α-helix (including 3–10 helices), β-sheet (both parallel and antiparallel) and turn were averaged over the time frame of analysis.

MM/PBSA per-residue energy decomposition

Free energy of binding ($\Delta G_{\mathrm{binding}}$) quantifies how favorable or unfavorable it is for a ligand to go from the solvated state to the receptor-bound state and can be broken down into the accompanying changes in enthalpic (ΔH) and entropic (ΔS) energy [Eq. (2)]. T denotes the temperature. The more negative the free energy, the more favorable is the binding between ligand and receptor relative to their existence free in solution.

$$\Delta G_{\mathrm{binding}} = \Delta H - T\Delta S \quad (2)$$

In the MM/PBSA approach [53], a combination of several methods is applied to obtain values for ΔH and ΔS and thereby $\Delta G_{\mathrm{binding}}$, according to the following relationship:

$$\Delta G_{\mathrm{binding}} = \left(\Delta E_{\mathrm{MM}} + \Delta G_{\mathrm{PB}} + \Delta G_{\mathrm{non\text{-}polar}}\right) - T\Delta S \quad (3)$$

where ΔE_{MM} is the molecular mechanics energy, ΔG_{PB} is the Poisson–Boltzmann energy and $\Delta G_{non\text{-}polar}$ is the non-polar solvation energy. The two latter terms can collectively be referred to as ΔG_{PBSA}. ΔE_{MM} encompasses terms for internal, van der Waals and coloumbic energies and can be calculated using a molecular mechanics force field. Representative conformational ensembles of the ligand, receptor and complex to be subjected to MM/PBSA analysis are often generated in explicit solvent MD simulations. Water and ions are stripped from the snapshots and replaced by an implicit continuum model before the calculations. We applied the single trajectory protocol, in which all the structures are derived from the complex trajectory [53–57].

In the MM/PBSA part of this study, our objectives were to identify residues important for binding of TH peptides to 14-3-3γ and to the POPS membrane and to evaluate differences between TH-(1-43) and THp-(1-43) with regard to membrane binding. For this reason and because of the high computational costs related to entropy calculations, we chose to focus on the enthalpic contribution and disregard the entropic term ($T\Delta S$) in Eq. (3):

$$\Delta G' = \Delta H = \Delta E_{MM} + \Delta G_{PB} + \Delta G_{non\text{-}polar} \quad (4)$$

The single quotation mark in $\Delta G'$ serves the purpose of differentiating the enthalpic free energy from the binding free energy [Eq. (3)]. The non-polar portion of the solvation free energy was estimated by linearly relating it to the solvent-accessible surface area (SASA):

$$\Delta G_{non\text{-}polar} = \gamma \mathrm{SASA} + \beta \quad (5)$$

A solvent probe of radius 1.4 Å was applied in order to derive SASA values. In accordance with the Parse parameter set [58], the regression coefficient γ and offset parameter β were set to 0.00542 and 0.92 kcal/mol, respectively. The electrostatic contribution to the solvation free energy (ΔG_{PB}) was calculated by solving the Poisson–Boltzmann equation with a maximum of 1000 iterations per snapshot. The internal dielectric constant was 1 while the external counterpart was 80 in the calculations. A grid spacing of 0.5 Å was used, along with a ratio of 4.0 between the longest dimension of the grid and that of the solute. Ionic strength was set to 150 mM, which approximately corresponds to physiological salt concentrations. Analyses were performed using the MMPBSA.py program incorporated into AmberTools 1.5 [44]. The script allows for the binding enthalpy $\Delta G'$ [Eq. (4)] to be decomposed into the contributions made by each residue in the system, in our case, individual residues in the TH peptides and 14-3-3γ, and individual POPS lipids. Prior to analysis, radii in the topology files were converted to the Parse variant [58]. We subjected 1000 conformations extracted evenly from the last 100 ns from each of the peptide:membrane simulations (Systems D and E in Table 2) to MM/PBSA per-residue decomposition analysis. In order to reduce the computational cost, only the peptide-interacting monolayer (i.e., 64 lipid molecules) comprised the receptor in the calculations. In terms of the 14-3-3γ:peptide system (System A in Table 2), 1000 frames were taken with equally spaced time steps from the last 50 ns of simulation. The 14-3-3γ:THp complex was divided into two ligand:receptor pairs for the MM/PBSA analysis, with each 14-3-3γ monomer representing the receptor and the bound peptide fragment regarded as the ligand in each case. The sets of snapshots represent satisfactorily equilibrated systems, as demonstrated by stable RMSD values (Figs. S2 and S3). Secondly, the time windows between frames (100 ps and 50 ps, respectively) are large enough to ensure that the snapshots are independent. The number of frames chosen was based on an attempt to reasonably balance statistical sample size and computational demand.

Acknowledgements

The authors would like to thank The Norwegian Research Council, The Kristian Gerhard Jebsen Foundation, Western Norway Health Authorities and the Meltzer fund for funding. This work was also supported by the National Institutes of Health Roadmap Grant GM073197 (to M.M. and R.C.S.). We thank the Amber community for support and advice. Notur and uniComputing are acknowledged for providing resources for computational studies.

Appendix A. Supplementary data

Supplementary data to this article can be found online at http://dx.doi.org/10.1016/j.jmb.2013.09.012.

Received 26 June 2013;
Received in revised form 27 August 2013;
Accepted 11 September 2013
Available online 17 September 2013

Keywords:
X-ray crystallography;
molecular dynamics simulations;
phospholipid bilayers;
phosphorylation;
free energy of binding

†Present address: Å. A. Skjevik, San Diego Supercomputer Center, University of California San Diego, 9500 Gilman Drive MC0505, La Jolla, CA 92093, USA.

Abbreviations used:
PC, phosphatidylcholine; POPS, palmitoyl-oleoyl phosphatidylserine; RU, response units; SPR, surface plasmon resonance; TH, tyrosine hydroxylase; MD, molecular dynamics; MM/PBSA, molecular mechanics Poisson–Boltzmann surface area.

References

[1] Aumann T, Horne M. Activity-dependent regulation of the dopamine phenotype in substantia nigra neurons. J Neurochem 2012;121:497–515.

[2] Daubner SC, Le T, Wang S. Tyrosine hydroxylase and regulation of dopamine synthesis. Arch Biochem Biophys 2011;508:1–12.

[3] Dunkley PR, Bobrovskaya L, Graham ME, von Nagy-Felsobuki EI, Dickson PW. Tyrosine hydroxylase phosphorylation: regulation and consequences. J Neurochem 2004;91:1025–43.

[4] Wang S, Sura GR, Dangott LJ, Fitzpatrick PF. Identification by hydrogen/deuterium exchange of structural changes in tyrosine hydroxylase associated with regulation. Biochemistry 2009;48:4972–9.

[5] Wang S, Lasagna M, Daubner SC, Reinhart GD, Fitzpatrick PF. Fluorescence spectroscopy as a probe of the effect of phosphorylation at serine 40 of tyrosine hydroxylase on the conformation of its regulatory domain. Biochemistry 2011;50:2364–70.

[6] Nakashima A, Mori K, Suzuki T, Kurita H, Otani M, Nagatsu T, et al. Dopamine inhibition of human tyrosine hydroxylase type 1 is controlled by the specific portion in the N-terminus of the enzyme. J Neurochem 1999;72:2145–53.

[7] Nakashima A, Hayashi N, Mori K, Kaneko YS, Nagatsu T, Ota A. Positive charge intrinsic to Arg(37)-Arg(38) is critical for dopamine inhibition of the catalytic activity of human tyrosine hydroxylase type 1. FEBS Lett 2000;465:59–63.

[8] Ichimura T, Isobe T, Okuyama T, Takahashi N, Araki K, Kuwano R, et al. Molecular cloning of cDNA coding for brain-specific 14-3-3 protein, a protein kinase-dependent activator of tyrosine and tryptophan hydroxylases. Proc Natl Acad Sci USA 1988;85:7084–8.

[9] Obsilova V, Nedbalkova E, Silhan J, Boura E, Herman P, Vecer J, et al. The 14-3-3 protein affects the conformation of the regulatory domain of human tyrosine hydroxylase. Biochemistry 2008;47:1768–77.

[10] Gordon SL, Bobrovskaya L, Dunkley PR, Dickson PW. Differential regulation of human tyrosine hydroxylase isoforms 1 and 2 in situ: isoform 2 is not phosphorylated at Ser35. Biochim Biophys Acta 2009;1793:1860–7.

[11] Salvatore MF, Pruett BS. Dichotomy of tyrosine hydroxylase and dopamine regulation between somatodendritic and terminal field areas of nigrostriatal and mesoaccumbens pathways. PLoS One 2012;7:e29867.

[12] Kuczenski RT, Mandell AJ. Regulatory properties of soluble and particulate rat brain tyrosine hydroxylase. J Biol Chem 1972;247:3114–22.

[13] McGeer EG, McGeer PL, Wada JA. Distribution of tyrosine hydroxylase in human and animal brain. J Neurochem 1971;18:1647–58.

[14] Chen R, Wei J, Fowler SC, Wu JY. Demonstration of functional coupling between dopamine synthesis and its packaging into synaptic vesicles. J Biomed Sci 2003;10:774–81.

[15] Tsudzuki T, Tsujita M. Isoosmotic isolation of rat brain synaptic vesicles, some of which contain tyrosine hydroxylase. J Biochem 2004;136:239–43.

[16] Morita K, Hamano S, Oka M. Ionic factors affecting the association of tyrosine hydroxylase with chromaffin granules in the adrenal medullary cell. Neurochem Int 1994;25:403–11.

[17] Cartier EA, Parra LA, Baust TB, Quiroz M, Salazar G, Faundez V, et al. A biochemical and functional protein complex involving dopamine synthesis and transport into synaptic vesicles. J Biol Chem 2010;285:1957–66.

[18] Morita K, Teraoka K, Oka M. Interaction of cytoplasmic tyrosine hydroxylase with chromaffin granule. *In vitro* studies on association of soluble enzyme with granule membranes and alteration in enzyme activity. J Biol Chem 1987;262:5654–8.

[19] Thórólfsson M, Døskeland AP, Muga A, Martínez A. The binding of tyrosine hydroxylase to negatively charged lipid bilayers involves the N-terminal region of the enzyme. FEBS Lett 2002;519:221–6.

[20] Bucciantini M, Cecchi C. Biological membranes as protein aggregation matrices and targets of amyloid toxicity. Methods Mol Biol 2010;648:231–43.

[21] Anderluh G, Lakey JH. Disparate proteins use similar architectures to damage membranes. Trends Biochem Sci 2008;33:482–90.

[22] Halskau O, Ying M, Baumann A, Kleppe R, Rodriguez-Larrea D, Almas B, et al. Three-way interaction between 14-3-3 proteins, the N-terminal region of tyrosine hydroxylase, and negatively charged membranes. J Biol Chem 2009;284:32758–69.

[23] Yang X, Lee WH, Sobott F, Papagrigoriou E, Robinson CV, Grossmann JG, et al. Structural basis for protein–protein interactions in the 14-3-3 protein family. Proc Natl Acad Sci USA 2006;103:17237–42.

[24] Yaffe MB, Rittinger K, Volinia S, Caron PR, Aitken A, Leffers H, et al. The structural basis for 14–3–3: phosphopeptide binding specificity. Cell 1997;91:961–71.

[25] Gardino AK, Smerdon SJ, Yaffe MB. Structural determinants of 14-3-3 binding specificities and regulation of subcellular localization of 14-3-3-ligand complexes: a comparison of the X-ray crystal structures of all human 14-3-3 isoforms. Semin Cancer Biol 2006;16:173–82.

[26] Obsil T, Obsilova V. Structural basis of 14-3-3 protein functions. Semin Cell Dev Biol 2011;22:663–72.

[27] Aitken A. 14-3-3 proteins: a historic overview. Semin Cancer Biol 2006;16:162–72.

[28] Goodwill KE, Sabatier C, Marks C, Raag R, Fitzpatrick PF, Stevens RC. Crystal structure of tyrosine hydroxylase at 2.3 Å and its implications for inherited neurodegenerative diseases. Nat Struct Biol 1997;4:578–85.

[29] Murphy KL, Zhang X, Gainetdinov RR, Beaulieu JM, Caron MG. A regulatory domain in the N terminus of tryptophan hydroxylase 2 controls enzyme expression. J Biol Chem 2008;283:13216–24.

[30] Torrente MP, Gelenberg AJ, Vrana KE. Boosting serotonin in the brain: is it time to revamp the treatment of depression? J Psychopharmacol 2012;26:629–35.

[31] Winge I, McKinney JA, Knappskog PM, Haavik J. Characterization of wild-type and mutant forms of human tryptophan hydroxylase 2. J Neurochem 2007;100:1648–57.

[32] Kabsch W. Automatic processing of rotation diffraction data from crystals of initially unknown symmetry and cell constants. J Appl Crystallogr 1993;26:795–800.

[33] Emsley P, Cowtan K. Coot: model-building tools for molecular graphics. Acta Crystallogr Sect D Biol Crystallogr 2004;60:2126–32.
[34] Collaborative Computational Project, Number 4. The CCP4 suite: programs for protein crystallography. Acta Crystallogr Sect D Biol Crystallogr 1994;50:760–3.
[35] Bohm G, Muhr R, Jaenicke R. Quantitative analysis of protein far UV circular dichroism spectra by neural networks. Protein Eng 1992;5:191–5.
[36] Accelrys Software Inc., D. S. M. E., Release 3.1. Discovery Studio Modeling Environment Release 3.1 edit. San Diego, CA: Accelrys Software Inc.; 2012.
[37] Mukhopadhyay P, Monticelli L, Tieleman DP. Molecular dynamics simulation of a palmitoyl-oleoyl phosphatidylserine bilayer with Na^+ counterions and NaCl. Biophys J 2004;86:1601–9.
[38] Frisch MJ, Trucks GW, Schlegel HB, Scuseria GE, Robb MA, Cheeseman JR, et al. Gaussian 03 Revision B. 05 edit. Pittsburgh PA: Gaussian, Inc.; 2003.
[39] Bayly CI, Cieplak P, Cornell WD, Kollman PA. A well-behaved electrostatic potential based method using charge restraints for deriving atomic charges: the RESP model. J Phys Chem 1993;97:10269–80.
[40] Wang J, Wang W, Kollman PA, Case DA. Automatic atom type and bond type perception in molecular mechanical calculations. J Mol Graphics Modell 2006;25:247–60.
[41] Wang J, Wolf RM, Caldwell JW, Kollman PA, Case DA. Development and testing of a general amber force field. J Comput Chem 2004;25:1157–74.
[42] Skjevik ÅA, Haug BE, Lygre H, Teigen K. Intramolecular hydrogen bonding in articaine can be related to superior bone tissue penetration: a molecular dynamics study. Biophys Chem 2011;154:18–25.
[43] Martínez L, Andrade R, Birgin EG, Martínez JM. PACKMOL: a package for building initial configurations for molecular dynamics simulations. J Comput Chem 2009;30:2157–64.
[44] Case DA, Darden TA, Cheatham TE, Simmerling CL, Wang J, Duke RE, et al. AMBER 11. San Francisco, CA: University of California; 2010.
[45] Darden T, York D, Pedersen L. Particle mesh Ewald: an *N*log(*N*) method for Ewald sums in large systems. J Chem Phys 1993;98:10089–92.
[46] Essmann U, Perera L, Berkowitz ML, Darden T, Lee H, Pedersen LG. A smooth particle mesh Ewald method. J Chem Phys 1995;103:8577–93.
[47] Ryckaert J-P, Ciccotti G, Berendsen HJC. Numerical integration of the cartesian equations of motion of a system with constraints: molecular dynamics of *n*-alkanes. J Comput Phys 1977;23:327–41.
[48] Loncharich RJ, Brooks BR, Pastor RW. Langevin dynamics of peptides: the frictional dependence of isomerization rates of *N*-acetylalanyl-*N*′-methylamide. Biopolymers 1992;32:523–35.
[49] Hornak V, Abel R, Okur A, Strockbine B, Roitberg A, Simmerling C. Comparison of multiple Amber force fields and development of improved protein backbone parameters. Proteins 2006;65:712–25.
[50] Homeyer N, Horn AHC, Lanig H, Sticht H. AMBER force-field parameters for phosphorylated amino acids in different protonation states: phosphoserine, phosphothreonine, phosphotyrosine, and phosphohistidine. J Mol Model 2006;12:281–9.
[51] Jorgensen WL, Chandrasekhar J, Madura JD, Impey RW, Klein ML. Comparison of simple potential functions for simulating liquid water. J Chem Phys 1983;79:926–35.
[52] Kabsch W, Sander C. Dictionary of protein secondary structure: pattern recognition of hydrogen-bonded and geometrical features. Biopolymers 1983;22:2577–637.
[53] Kollman PA, Massova I, Reyes C, Kuhn B, Huo S, Chong L, et al. Calculating structures and free energies of complex molecules: combining molecular mechanics and continuum models. Acc Chem Res 2000;33:889–97.
[54] Hou T, Wang J, Li Y, Wang W. Assessing the performance of the MM/PBSA and MM/GBSA methods. 1. The accuracy of binding free energy calculations based on molecular dynamics simulations. J Chem Inf Model 2011;51:69–82.
[55] Kar P, Knecht V. Origin of decrease in potency of darunavir and two related antiviral inhibitors against HIV-2 compared to HIV-1 protease. J Phys Chem B 2012;116:2605–14.
[56] Kar P, Lipowsky R, Knecht V. Importance of polar solvation for cross-reactivity of antibody and its variants with steroids. J Phys Chem B 2011;115:7661–9.
[57] Lafont V, Schaefer M, Stote RH, Altschuh D, Dejaegere A. Protein–protein recognition and interaction hot spots in an antigen–antibody complex: free energy decomposition identifies "efficient amino acids". Proteins 2007;67:418–34.
[58] Sitkoff D, Sharp KA, Honig B. Accurate calculation of hydration free energies using macroscopic solvent models. J Phys Chem 1994;98:1978–88.
[59] Xu C, Jin J, Bian C, Lam R, Tian R, Weist R, et al. Sequence-specific recognition of a PxLPxl/L motif by an ankyrin repeat tumbler lock. Sci Signal 2012;5:ra39.
[60] Obsilova V, Herman P, Vecer J, Sulc M, Teisinger J, Obsil T. 14-3-3ζ C-terminal stretch changes its conformation upon ligand binding and phosphorylation at Thr232. J Biol Chem 2004;279:4531–40.
[61] Silhan J, Obsilova V, Vecer J, Herman P, Sulc M, Teisinger J, et al. 14-3-3 protein C-terminal stretch occupies ligand binding groove and is displaced by phosphopeptide binding. J Biol Chem 2004;279:49113–9.
[62] Liu D, Bienkowska J, Petosa C, Collier RJ, Fu H, Liddington R. Crystal structure of the zeta isoform of the 14-3-3 protein. Nature 1995;376:191–4.
[63] Xiao B, Smerdon SJ, Jones DH, Dodson GG, Soneji Y, Aitken A, et al. Structure of a 14-3-3 protein and implications for coordination of multiple signalling pathways. Nature 1995;376:188–91.
[64] Kalita DJ, Kumar A, Kumar S. Structure–function studies of *Bubalus bubalis* lingual antimicrobial peptide analogs. Vet Res Commun 2009;33:149–61.
[65] Greenfield NJ. Using circular dichroism spectra to estimate protein secondary structure. Nat Protoc 2006;1:2876–90.
[66] Miranda FF, Teigen K, Thorolfsson M, Svebak RM, Knappskog PM, Flatmark T, et al. Phosphorylation and mutations of Ser(16) in human phenylalanine hydroxylase. Kinetic and structural effects. J Biol Chem 2002;277:40937–43.
[67] Stultz CM, Levin AD, Edelman ER. Phosphorylation-induced conformational changes in a mitogen-activated protein kinase substrate. Implications for tyrosine hydroxylase activation. J Biol Chem 2002;277:47653–61.
[68] Rodland I, Halskau O, Martinez A, Holmsen H. α-Lactalbumin binding and membrane integrity—effect of charge and degree of unsaturation of glycerophospholipids. Biochim Biophys Acta 2005;1717:11–20.
[69] Winge I, McKinney JA, Ying M, D'Santos CS, Kleppe R, Knappskog PM, et al. Activation and stabilization of human tryptophan hydroxylase 2 by phosphorylation and 14-3-3 binding. Biochem J 2008;410:195–204.

[70] Xue B, Dunbrack RL, Williams RW, Dunker AK, Uversky VN. PONDR-FIT: a meta-predictor of intrinsically disordered amino acids. Biochim Biophys Acta 2010;1804:996–1010.
[71] Sickmeier M, Hamilton JA, LeGall T, Vacic V, Cortese MS, Tantos A, et al. DisProt: the Database of Disordered Proteins. Nucleic Acids Res 2007;35:D786–93.
[72] Kovacs D, Szabo B, Pancsa R, Tompa P. Intrinsically disordered proteins undergo and assist folding transitions in the proteome. Arch Biochem Biophys 2013;531:80–9.
[73] Obsil T, Ghirlando R, Klein DC, Ganguly S, Dyda F. Crystal structure of the 14-3-3ζ:serotonin *N*-acetyltransferase complex. a role for scaffolding in enzyme regulation. Cell 2001;105:257–67.